Front. Earth Sci. 2023, 17(2): 547–560
https://doi.org/10.1007/s11707-022-1008-z

RESEARCH ARTICLE

The north-east North Atlantic Tripole implicated as a predictor of the August precipitation decadal variability over north China

Tiejun XIE[1], Ji WANG[1], Peiqun ZHANG[2], Taichen FENG[3], Xiaoxiao ZHANG[1], Yingjuan ZHANG (✉)[1]

1 Beijing Municipal Climate Center, Beijing Meteorological Bureau, Beijing 100089, China
2 National Climate Center, China Meteorological Administration, Beijing 100081, China
3 Key Laboratory for Semi-Arid Climate Change of the Ministry of Education, College of Atmospheric Sciences, Lanzhou University, Lanzhou 730000, China

Abstract Monthly precipitation over north China in August (NCAP) is the second highest in the year, and it is important to understand its driving mechanisms to facilitate reliable forecasting. The NCAP displays a significant decadal variability of a cycle about 10-year and negatively correlates with the July north-east North Atlantic Tripole (NAT) over the decadal timescales. This study shows that the Eurasian decadal teleconnection (EAT) acts as a bridge that links the July NAT with NCAP decadal variability. This coupled ocean–atmosphere bridge (COAB) mechanism, through which the July NAT influences the decadal variability of NCAP, can be summarized as follows. The cumulative effect of the NAT drives the EAT to adjust atmospheric circulation over north China and the surrounding regions, and so regulates precipitation in north China by influencing local water vapor transport. When the July NAT is in a negative (positive) phase, the EAT pattern has a positive (negative) pattern, which promotes (weakens) the transmission of water vapor from the sea in the south-east to north China, thus increasing (decreasing) NCAP over decadal timescales. The decadal NCAP model established based on the July NAT can effectively predict the NCAP decadal variability, illustrating that the July NAT can be implicated as a predictor of the NCAP decadal variability.

Keywords north China August precipitation (NCAP), north-east North Atlantic Tripole (NAT), Eurasian decadal teleconnection (EAT) pattern, coupled oceanic-atmospheric bridge (COAB), decadal variability

Received January 10, 2022; accepted May 9, 2022

E-mail: zhangyj@bj.cma.gov.cn

1 Introduction

Most precipitation in north China (34°N–44°N, 110°E–120°E) occurs in July and August, with these months accounting for more than half of the total annual precipitation (Hao and Ding, 2012). The amount of precipitation in August is second only to the amount in July, but the precipitation in these two months follows different decadal cycles (Lu, 1999). High precipitation in July and August can have a serious effect on urban activity and agricultural production; however, low precipitation in July and August can also have a serious impact. Prediction of north China August precipitation (NCAP) is therefore important, as it provides useful information for government mitigation planning and water resource regulation.

Previous research into summer precipitation in north China has generally focused on June to August as a single period, and monthly-scale precipitation in summer has received little attention, with the exception of a few case studies (e.g., Liu et al., 1992; Li et al., 2002; Dai et al., 2003; Fu and Zeng, 2005; Fan et al., 2009; Sun et al., 2018; Zhao et al., 2020). Lu (1999) found that the decadal variability of precipitation in north China in July differs from that in August. Using the most recent data available, we found that July precipitation in north China follows an approximately 20-year cycle, whereas precipitation in August follows an approximately 10-year cycle. This suggests that the mechanisms that drive the decadal variability of precipitation over north China may be different for July and August.

Previous research has shown that summer precipitation over north China is affected by local climate factors, such as the East Asian summer monsoon (EASM; Zhu and Wang, 2001; Zhang et al., 2003; Huang et al., 2007; Ding et al., 2008; Jiang et al., 2008; Wang et al., 2008; Zhang,

2015; Zhao et al., 2016), the South Asian High (Jiang et al., 2011; Wei, 2012; Choi et al., 2016), and the West Pacific Subtropical High (WPSH; Xu et al., 2005; Mao and Wu, 2006; Sun et al., 2009), and by climate factors from nearby areas such as the Indian summer monsoon (Zhang, 1999; Wei et al., 2014; Bueh et al., 2016; Wu and Jiao, 2017), the El Niño–Southern Oscillation (ENSO; Wu et al., 2003; Xue and Liu, 2008; Lin and Lu, 2009), and tropical cyclones (Chen et al., 2019). The decadal variability of precipitation over north China may be closely related to the upper mid-high latitude circulation system (Li and Li, 2000; Lu et al., 2006; Fu et al., 2009; Li et al., 2013; Xie et al., 2021). The North Atlantic is at the upstream end of the mid-high latitude circulation system that affects north China, which suggests that decadal precipitation variability in north China may be influenced by the North Atlantic climate.

The North Atlantic climate includes features such as the North Atlantic Oscillation (NAO), the Atlantic multidecadal oscillation (AMO), the Atlantic meridional overturning circulation (AMOC), and the North Atlantic Tripole (NAT). Delayed-oscillator model simulations of the NAO show that these climate features are interdependent; for example, a positive AMO can affect ocean heat transport via the AMOC and resulting in negative NAT-type sea surface temperature (SST) anomalies with a time delay of 15–20 years and can have a significant impact on the climate in East Asia (Sun et al., 2015; Li et al., 2022). Wu et al. (2009) found that an anomalous NAO in spring can influence the EASM by affecting SSTs in the North Atlantic to create the East Asian subtropical front. Zuo et al. (2013) found that the North Atlantic SST tripole can influence the EASM in summer, which is a driver for precipitation in north China. Li et al. (2018) found that spring precipitation in South-west China is positively related to SSTs in the North Atlantic and can affect spring precipitation in South-west China via an atmospheric bridge. Han and Zhang (2022) found a significant positive correlation between spring precipitation in the middle and lower reaches of the Yangtze River Valley and the NAO in the preceding winter. Our study shows that NCAP decadal variability may also be related to SSTs in the northeastern North Atlantic, hereafter referred to as the northeast NAT.

In this paper, we investigate the dynamic links between the July NAT and NCAP over decadal timescales and establish an empirical model of NCAP decadal variability driven by the July NAT. The paper is organized as follows: Section 2 describes the data and methodology used in this study; Section 3 shows the decadal variability of NCAP and its relationship with the July NAT; Section 4 analyzes the dynamic links between the NAT and NCAP; we establish an empirical model of NACP decadal variability driven by the July NAT in Section 5; and a summary and discussion are presented in Section 6.

2 Data and methodology

2.1 Data sets

We use precipitation data for 1979–2021 from the Global Precipitation Climatology Project (GPCP) Version 2.3 Combined Precipitation Data set at a resolution of 2.5° × 2.5° (Adler et al., 2003), which captures the characteristics of precipitation in north China well, and we use wind, geopotential height, and relative humidity for 1979–2021 from the NCEP–DOE (US National Centers for Environmental Predictions–Department of Energy) reanalysis 2 data set at a resolution of 2.5° × 2.5° (Kanamitsu et al., 2002). The SST data used in our study are from the Hadley Centre Sea Ice and Sea Surface Temperature (HadISST) data set, which has a resolution of 1° × 1° and covers the period 1870–2021 (Rayner et al., 2003).

2.2 Indices

We use area-weighted mean August precipitation anomalies, relative to the base period 1979–2010, to construct an NCAP time series for our study region in north China (34°N–44°N, 110°E–120°E).

The NAT is defined as follows:

$$\mathrm{NAT} = \frac{1}{2}\left[\frac{A_1^*+A_3^*}{2} - A_2^*\right], \tag{1}$$

where A_1^*, A_2^*, and A_3^* are the normalized area-weighted SST anomalies for the areas A_1 [30°N–40°N, 40°W–30°W], A_2 [50°N–60°N, 25°W–15°W], and A_3 [65°N–75°N, 3°E–13°E], respectively.

The August Eurasian decadal teleconnection index (EAT) is the normalized difference of the geopotential height anomalies at 500 hPa for the four regions of action in August calculated by

$$\mathrm{EAT} = \frac{1}{2}\left[\frac{B_1^*+B_2^*}{2} - \frac{B_3^*+B_4^*}{2}\right], \tag{2}$$

where B_1^*, B_2^*, B_3^*, and B_4^* are the normalized area-weighted 500 hPa geopotential height anomalies for the areas B_1 [60°N–70°N, 24°W–16°W], B_2 [42°N–52°N, 10°E–20°E], B_3 [50°N–60°N, 50°E–60°E], and B_4 [42°N–48°N, 100°E–108°E], respectively.

2.3 Dynamic diagnosis

In this paper, we use wave activity analysis to analyze the stationary Rossby wave energy propagation, and we calculate the wave activity flux following Takaya and Nakamura (2001):

$$W=\frac{p\cos\varphi}{2|U|}\cdot\begin{Bmatrix}\dfrac{U}{a^2\cos^2\varphi}\left[\left(\dfrac{\partial\psi'}{\partial\lambda}\right)^2-\psi'\dfrac{\partial^2\psi'}{\partial\lambda^2}\right]+\dfrac{V}{a^2\cos\varphi}\left[\dfrac{\partial\psi'}{\partial\lambda}\dfrac{\partial\psi'}{\partial\varphi}-\psi'\dfrac{\partial^2\psi'}{\partial\lambda\partial\varphi}\right]\\ \dfrac{U}{a^2\cos\varphi}\left[\dfrac{\partial\psi'}{\partial\lambda}\dfrac{\partial\psi'}{\partial\varphi}-\psi'\dfrac{\partial^2\psi'}{\partial\lambda\partial\varphi}\right]+\dfrac{V}{a^2}\left[\left(\dfrac{\partial\psi'}{\partial\varphi}\right)^2-\psi'\dfrac{\partial^2\psi'}{\partial\varphi^2}\right]\\ \dfrac{f_0^2}{N^2}\left\{\dfrac{U}{a\cos\varphi}\left[\dfrac{\partial\psi'}{\partial\lambda}\dfrac{\partial\psi'}{\partial z}-\psi'\dfrac{\partial^2\psi'}{\partial\lambda\partial z}\right]+\dfrac{V}{a}\left[\dfrac{\partial\psi'}{\partial\varphi}\dfrac{\partial\psi'}{\partial z}-\psi'\dfrac{\partial^2\psi'}{\partial\varphi\partial z}\right]\right\}\end{Bmatrix}, \tag{3}$$

where p, U, φ, λ, a, and f_0 denote the pressure, basic flow, latitude, longitude, Earth's radius and Coriolis parameter, respectively; and $z=-H\ln p$, where H is a constant scale height. The buoyancy frequency squared can be calculated as follows:

$$N^2=\frac{R_a p^{\kappa}}{H}\cdot\frac{\partial\theta}{\partial z}, \tag{4}$$

where R_a and θ denote the gas constant of dry air and the potential temperature, respectively; and κ denotes normalized R_a based on the specific heat of air for constant pressure. The geostrophic stream function is defined as

$$\psi'=\frac{\phi}{f}, \tag{5}$$

where ϕ denotes geopotential, and ψ' denotes the disturbances for ψ.

The vertically integrated whole layer water vapor flux (Q) is calculated and the formula as follows:

$$Q=-\frac{1}{g}\int_{psfc}^{0}\left(q\vec{V}\right)\mathrm{d}p, \tag{6}$$

where g, $psfc$, q, $\vec{V}$, and p denote gravity, surface pressure, specific humidity, wind field and pressure, respectively. The q in each layer (q_l) is calculated as follows (Gill, 1982):

$$q_l=0.622\times\frac{e_l}{p_l-0.378e_l}, \tag{7}$$

where p_l and e_l denote the local pressure and water vapor pressure for l layer, respectively; and e_l is calculated as follows (Gill, 1982):

$$e_l=r_h 10^{\frac{0.7859+0.03477T_l}{1.0+0.004212T_l}+2}, \tag{8}$$

where r_h and T_l denote the local relative humidity and air temperature for l layer, respectively.

2.4 Statistical methods

A 7-year Gaussian low-pass filter is applied to highlight the decadal signals. Time series after low-pass filtered could have high autocorrelation so that the number of effective degrees of freedom (N^{eff}) is used and estimated as follows (Pyper and Peterman, 1998; Xie et al., 2021; Li et al., 2022):

$$\frac{1}{N^{\mathrm{eff}}}\approx\frac{1}{N}+\frac{2}{N}\sum_{j=1}^{N-2}\frac{N-j}{N}\rho_{XX}(j)\rho_{YY}(j), \tag{9}$$

where N is the sample size, $\rho_{XX}(j)$ and $\rho_{YY}(j)$ are the autocorrelations for two time series, X and Y, at lag j, respectively.

Some other statistical methods are also applied in this research, including: Gaussian low-pass filtering, continuous power spectrum analysis, wavelet power spectrum analysis, composite analysis, correlation and regression analysis and so on, and these details will not be described in detail here.

3 Decadal variability in NCAP and its relationship with the NAT

The time series for NCAP is shown in Fig. 1, which shows the NCAP anomaly superimposed on the multidecadal trend (blue line), with a decadal cycle (green line) of about 10 years. As shown in Fig. 4(a), after removing the multidecadal change trend, the decadal variability of the NCAP is more obvious. The NCAP anomaly was in a positive phase during 1982–1987, 1993–1997, 2005–2011, and 2018–2021, and it was in a negative phase during 1988–1992, 1998–2004, and 2012–2017, when considered over decadal timescales. Figure 2(a) shows that August precipitation over north China is significantly spatially consistent at decadal timescales. The decadal NCAP cycle is analyzed using

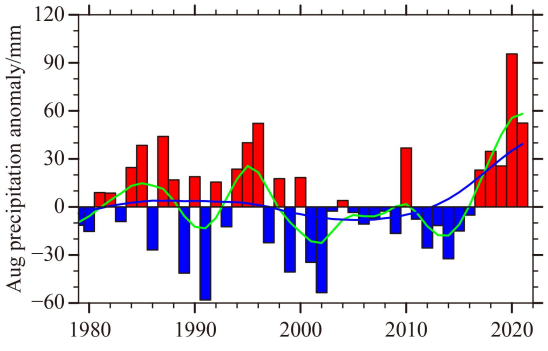

Fig. 1 Time series of annual NCAP anomalies. Area-weighted mean annual NCAP anomalies (bars) for 1979–2021, based on the GPCP data set. Solid green line and solid blue line are the annual NCAP anomalies after 7-year and 21-year low-pass Gaussian filtering, respectively.

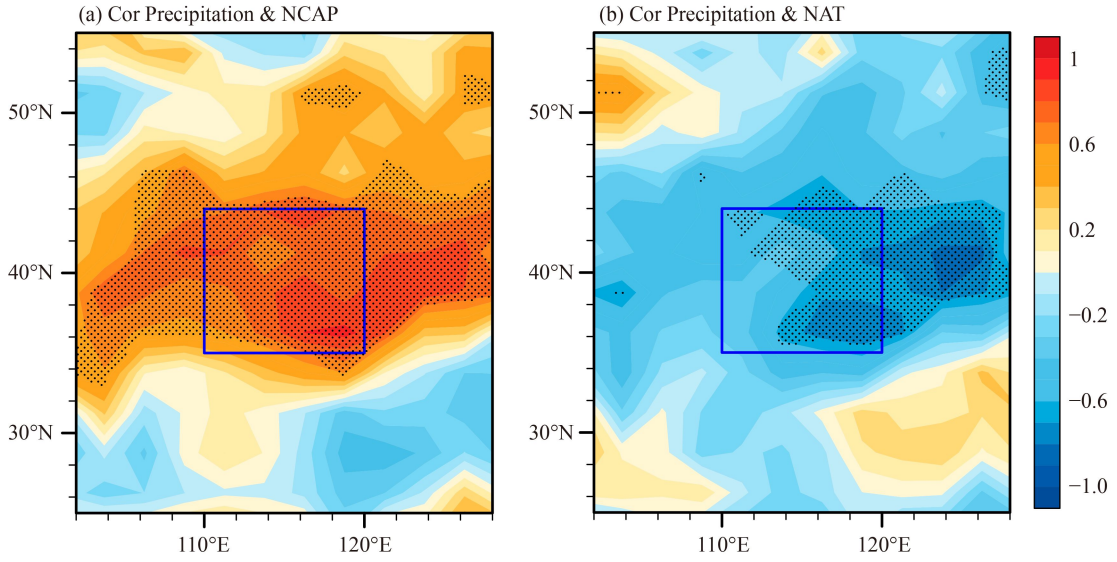

Fig. 2 Correlation coefficients of the August precipitation with the NCAP and NAT in north China. (a) Correlation between NCAP and August precipitation anomalies over north China and the surrounding region during 1979–2021 after 7-year Gaussian low-pass filtering. The researched north China region (35°–44°N, 110°–120°E) is surrounded by a blue box. The black dot indicates values significant values at the 95% confidence level using the effective number of degrees of freedom. (b) As in (a), but for the correlation coefficients of the August precipitation with the NAT index.

continuous power spectrum analysis and wavelet power spectrum analysis. As shown in Fig. 3, NCAP has a significant spectral peak on decadal cycle of 10-year, and this decadal cycle is significant from 1979 to the present. Previous research has also shown that NCAP has decadal variability with a 10-year cycle (e. g., Lu, 1999).

Similar to the NCAP, the July NAT index also has decadal variability with a 10-year cycle. As shown in Fig. 4(a), the July NAT index and NCAP show opposite phase relationship over decadal timescales: the July NAT was in a negative phase during 1981–1986, 1994–1999, 2005–2011, and 2018–2021, whereas the NCAP anomaly was positive during the same periods. The July NAT was in a positive phase during 1987–1993, 2001–2004, and 2012–2017 when the NCAP anomaly was negative. The correlation coefficient between the July NAT and NCAP is −0.783 over decadal timescales (at a confidence level exceeding 95%). The 17-year sliding-window correlation between the July NAT and the NCAP anomaly shows that the negative correlation between the July NAT and NCAP over decadal timescales is stable (Fig. 3(b)).

The spatial distribution of the correlation between the July NAT and decadal August precipitation variability over north China and the surrounding region was analyzed to explore the relationship between the July NAT and NCAP. Figure 5(b) shows that the correlation coefficient is stronger than −0.5 over almost all of north China, and it is stronger than −0.6 in eastern north China (which accounts for more than half of north China) and stronger than −0.7 in south-eastern north China. This is further evidence that there is a strong relationship between the July NAT and NCAP.

The above results illustrate that NCAP anomalies are significantly and negatively correlated with the July NAT

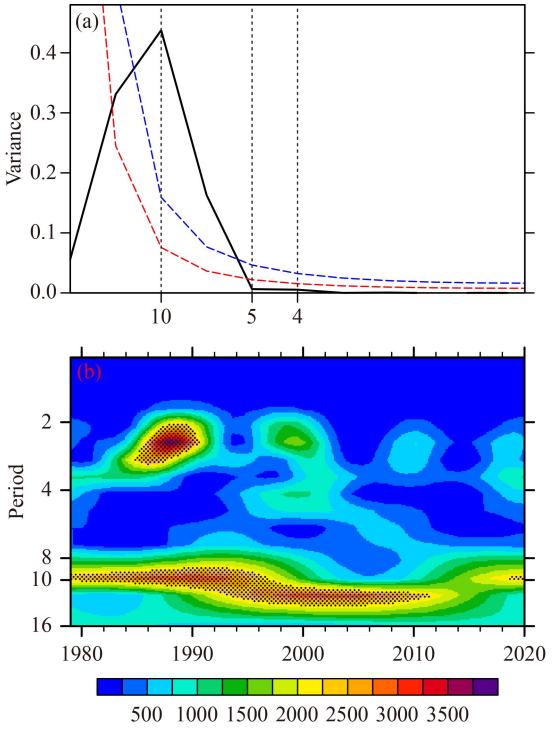

Fig. 3 Power spectrum and wavelet power spectrum of annual NCAP anomalies. (a) Power spectrum of annual NCAP anomalies for 1979–2021 over decadal timescales. The blue (red) dashed line is the reference red noise spectrum (at the 95% confidence level). (b) As in (a), but for wavelet power spectrum. The dotted area indicates the 95% confidence level.

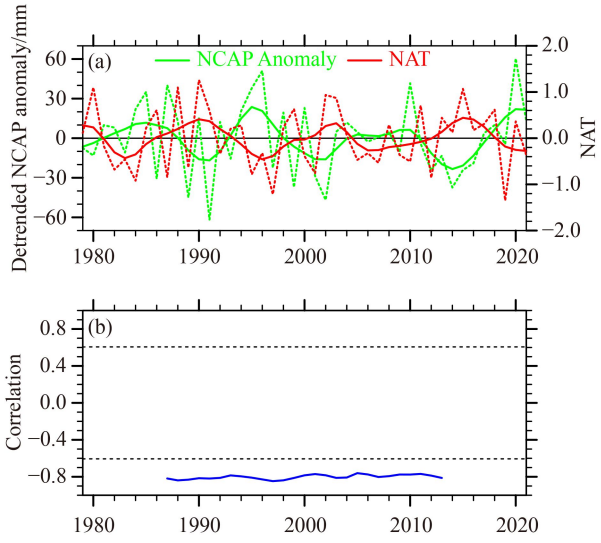

Fig. 4 Time series of the NAT and detrended NCAP anomalies and its sliding-window correlation. (a) The dashed green (red) line is the time series of the detrended NCAP anomalies (NAT index) for 1979–2021. The solid green and red lines are the decadal variability of the detrended NCAP anomalies and NAT index for 1979–2021. (b) The blue line is the 17-year sliding-window correlation between the NAT and detrended NCAP anomalies (1979–2021) over decadal timescales. The two dashed lines indicate the 99% confidence level, calculated using the effective number of degrees of freedom.

over decadal timescales, implying that the 10-year cycle for decadal NCAP variability may be influenced by the NAT. This suggests that it may be appropriate to use the July NAT as a predictor for decadal NCAP variability.

4 Dynamic links between the NAT and NCAP over decadal timescales

The climate variability with a longer timescale in north China is more commonly related to the atmosphere circulation at upper mid-high latitude (e.g., Li and Li, 2000; Lu et al., 2006; Fu et al., 2009; Li et al., 2013; Sun et al., 2017; Xie et al., 2019). Figure 5 shows the composite and composite difference for August geopotential height anomalies at 500 hPa, corresponding to NCAP decadal variability. The 500 hPa geopotential height field has a "positive–negative–positive–negative" structure over the North Atlantic–Eurasia region in August during periods when the NCAP anomalies are positive over decadal timescales. Iceland and the Ural Mountains are positive anomaly activity centers, and central Europe and Baikal Lake are negative anomaly activity centers. In north China, the geopotential height anomalies are negative in the north-west and positive in the south-east, and the positive anomaly activity center over the Sea of

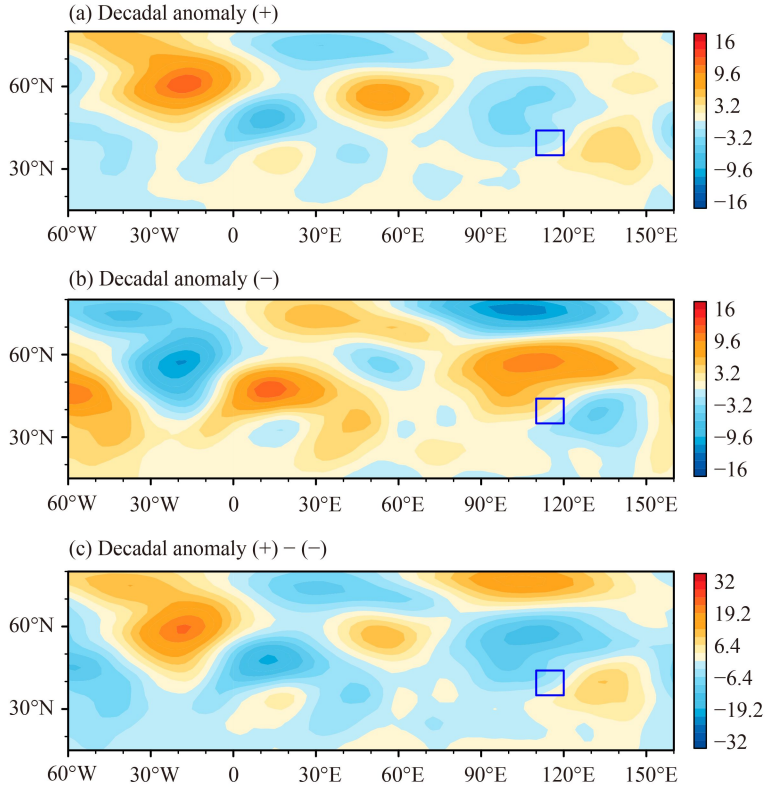

Fig. 5 Composite and composite difference of August geopotential height anomalies at 500 hPa corresponding to the NCAP anomalies. (a) Composite of August geopotential height anomalies at 500 hPa during the period when the NCAP is in positive phase over decadal timescales. (b) As in (a), but for the period when the NCAP is in negative phase. (c) As in (a), but for the composite difference between (a) and (b).

Japan corresponds to a stronger WPSH, which promotes the transmission of water vapor from the sea in the south-east to north China. In contrast, when the NCAP anomaly is negative over decadal timescales, the corresponding August geopotential height field has the opposite structure to that present when the NCAP anomaly is positive: it has a "negative–positive–negative–positive" structure from the North Atlantic to Eurasia; the geopotential height anomalies in north China are negative in the south-east and positive in the north-west; and the negative anomaly activity center over the Sea of Japan corresponds to a weaker WPSH, which weakens the transmission of water vapor from the sea in the south-east to north China (Fig. 5(b)). The composite difference between Fig. 5(a) and 5(b) is shown in Fig. 5(c), where the zonal structure of the August 500 hPa geopotential height anomalies corresponding to different phases of the NCAP decadal variability can be seen clearly.

The horizontal stationary wave activity flux corresponding to positive NCAP anomalies over decadal timescales is shown in Fig. 6(a). It can be seen that the divergence and convergence centers of the velocity potential correspond to the activity centers for the geopotential height anomalies in Fig. 5. The divergent wind suggests that the anomalous upper-level divergence that occurs over the North Atlantic may be transmitted to north China through the activity centers mentioned above. These indicate that there may be a Eurasian decadal teleconnection (EAT) pattern over the North Atlantic-Eurasia region, and the EAT may be the way NAT affects the NCAP decadal variability.

Next, the EAT pattern is defined (please see Section 2.2 for details) and the horizontal structure (Fig. 7(a)) and vertical structure (Fig. 7(b)) of the EAT patten in August are shown. The spatial structure of the EAT is significant both horizontally and vertically, characterized by a zonal wave structure with positive and negative anomaly centers extending alternately from the North Atlantic to East Asia through the activity centers of the EAT pattern. These results indicate that this EAT pattern is significant in August, and that the relationship between the EAT and NCAP decadal variability is corresponding: when the EAT is in a positive phase, the geopotential height anomalies are negative in northern north China and positive in the south, also corresponding to a stronger WPSH, which promotes the transmission of water vapor from the sea in the south-east to north China region; and vice versa. In addition, it should be noted that similar teleconnection was pointed out by Li and Ruan (2018) based on the summer average geopotential height field over northern hemisphere.

Figure 6(b) shows the horizontal stationary wave activity flux associated with the EAT pattern. It can be seen that the velocity potential and divergent wind anomalies associated with the EAT pattern almost consistent with that corresponding to the positive NCAP

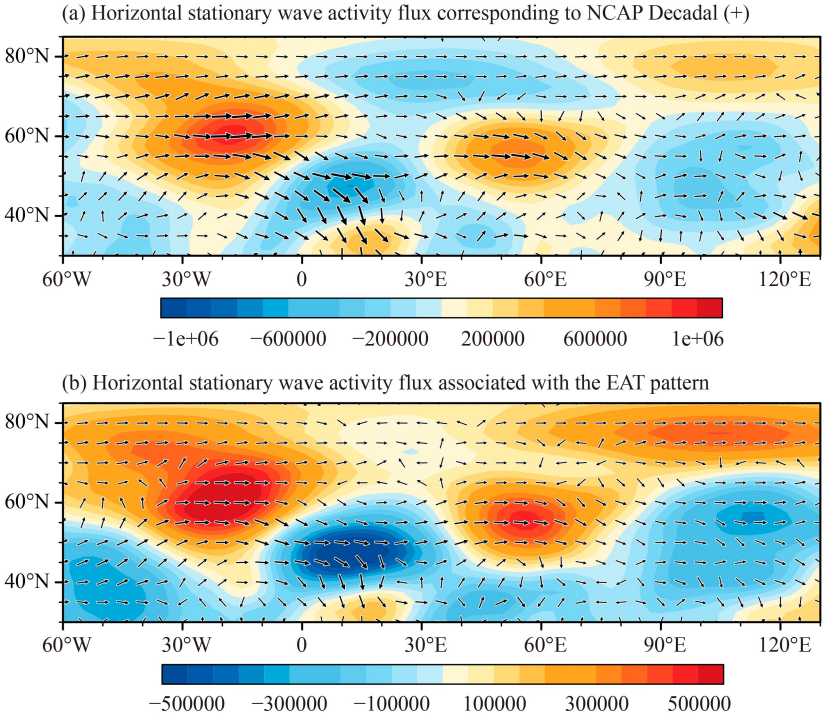

Fig. 6 Horizontal stationary wave activity flux corresponding to the NCAP positive anomalies and associated with the EAT pattern. (a) Horizontal stationary wave activity flux at 500 hPa corresponding to the NCAP positive anomalies over decadal timescales, based on T-N wave activity flux. Contours and vectors indicate the velocity potential and divergent wind anomalies, respectively. (b) As in (a), but associated with the EAT pattern.

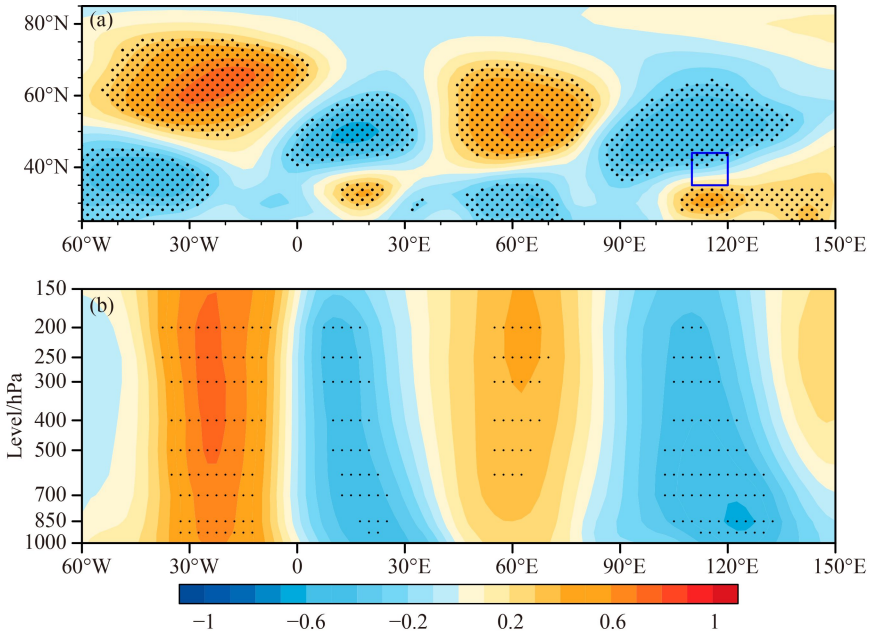

Fig. 7 The regression coefficients of 500 hPa geopotential height anomalies against EAT index. (a) Regression coefficients of the normalized 500 hPa geopotential height anomalies over the North Atlantic-Eurasia (35°N–85°N, 60°W–150°E) against the EAT index for 1979–2021. Dotted areas indicate regression coefficients significant above the 95% confidence level, calculated using the effective number of degrees of freedom. (b) As in (a), but in the vertical direction for the regression coefficients of mean values of geopotential height at 45°–65°N against the EAT index.

anomalies. This illustrates that most of the atmospheric circulation field affecting the NCAP decadal variability is related to the EAT, which further verifies the influence of the EAT on the decadal variability of NCAP.

Then, the linkage between the July NAT and the August EAT and the mechanism of the July NAT influencing the August EAT over decadal timescales were discussed. Figures 8(a) and 8(b) show the correlation map between the August EAT index and SST anomalies over the north-eastern North Atlantic in July and August, respectively. It can be seen that the correlation coefficients between the EAT and SST in north-eastern North Atlantic region over decadal timescales present a tripole pattern from the Azores to the Norwegian Sea in July, corresponding to the negative phase of the NAT pattern. This also corresponds to the relationship between the July NAT and NCAP over decadal timescales: the negative NAT–positive EAT–positive NCAP; and

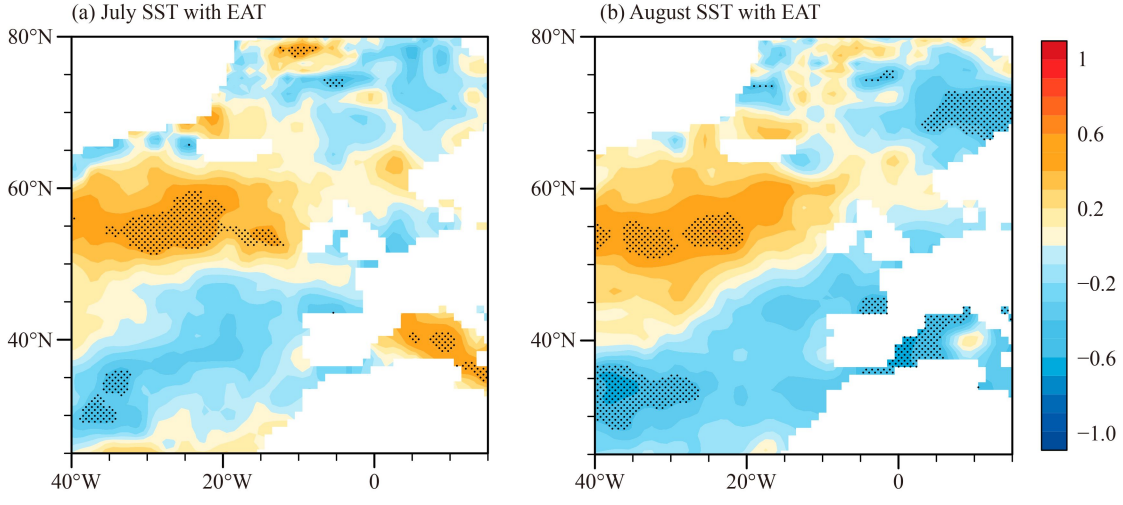

Fig. 8 Correlation coefficients between the EAT and SST. (a) Correlation coefficients between the EAT and detrended SST anomalies over the north-east Northern Atlantic over decadal timescales during 1979–2021. The dotted area indicates significant values above the 95% confidence level, calculated using the effective number of degrees of freedom. (b) as in (a), but using SST for August.

similarly, when the phases are opposite. This tripole pattern is enhanced in August. These results illustrate that the EAT is related to conditions in the NAT, and although the relationship in August is more significant than that in July, the August EAT can be effectively predicted in advance based on July NAT.

Figure 9(a) shows the coefficients for the regressions of the 500 hPa geopotential height and zonal-meridional wind over the north-east North Atlantic against the negative NAT [NAT(-)] over decadal timescales. It can be seen that the negative NAT pattern can stimulate an anticyclone anomaly in the north-eastern North Atlantic, which corresponds to the EAT activity center in the North Atlantic. Figure 9(b) shows the coefficients for the regressions of the geopotential height anomalies and vertical wind at 45°N–65°N over the activity center against the negative NAT over decadal timescales in the vertical direction. It can be seen that the negative NAT corresponds to an upward vertical wind anomaly in this activity center which is consistent with the result in Fig. 9(a). This circulation can be stimulated by the SSTs in the north-eastern North Atlantic has also been pointed out by another research (Li et al., 2018).

The lead-lag correlation between the July NAT, August EAT, and NCAP was used to further research the linkage from the July NAT to NCAP. As shown in Fig. 10(a), the lead-lag correlation coefficient between the July NAT and August EAT reaches its extreme value of –0.47 (exceeding 95% confidence level) when there is no lag over decadal timescales. Similarly, as shown in Fig. 10(b), the

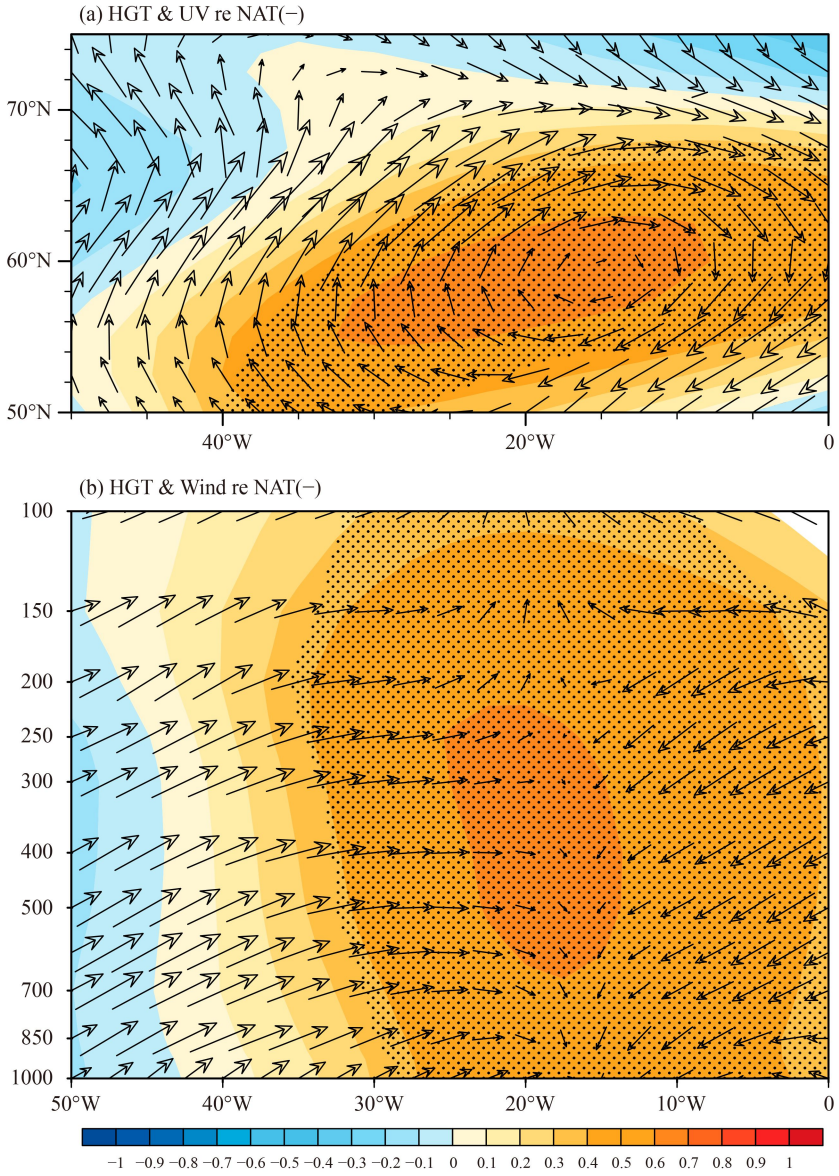

Fig. 9 The regression coefficients of geopotential height anomalies and wind against the negative NAT. (a) As in Fig. 7(a), but for the geopotential height anomalies and zonal-meridional wind over the north-eastern Atlantic onto the negative NAT [NAT(-)]. (b) As in Fig. 7(b), but over the north-eastern Atlantic.

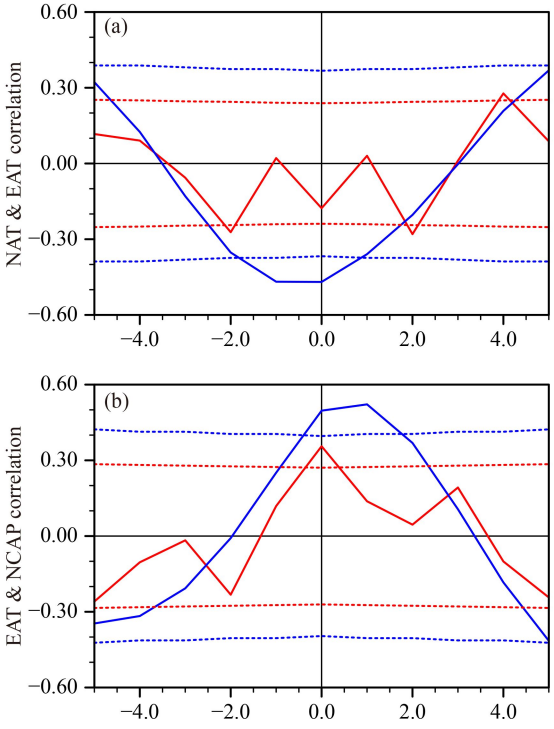

Fig. 10 Lead–lag correlation between July NAT, August EAT and NCAP. (a) Lead–lag correlation between the July NAT and detrended NCAP anomalies for 1979–2021. The red and blue solid lines are the correlation coefficients for the raw and 7-year low-pass Gaussian low-pass filtered time series, respectively. Negative (positive) lags indicate that the NAT leads (lags) the NCAP. The red and blue dashed lines are the 95% confidence levels corresponding to raw and Gaussian low-pass filtered time series, respectively. (b) As in (a), but for August EAT and NCAP.

lead-lag correlation coefficient between the August EAT and NCAP over decadal timescales is 0.50 (above the 95% confidence level) when there is no lag between the NCAP and the July EAT. These results further illustrate that the EAT is a bridge linking the July NAT and NCAP over decadal timescales, and that the July NAT can as a good predictor of NCAP decadal variability.

Furthermore, as shown in Fig. 11(a), the regression pattern of the 500 hPa zonal-meridional wind anomalies in August against the EAT index on decadal timescale is correspond to the composite difference of the 500 hPa geopotential height field associated with the NCAP decadal variability and EAT pattern. The positive phase of the EAT is conducive to water vapor transport from the sea in the south-east to north China. Figure 11(b) shows the pattern for the regression of the 500 hPa zonal-meridional wind anomalies in August against the negative NAT over decadal timescales. The negative phase of the NAT is conducive to water vapor transport from the south-east sea to north China. The pattern is not completely consistent with that regressed onto the EAT, illustrating that the NAT influences the NCAP decadal variability through the EAT. These results further verify the dynamical linkage of NAT-EAT-NCAP.

In addition, the composite of the whole layer vertically integrated water vapor flux anomalies corresponding to the NCAP anomalies and the composite difference are shown in Figs. 12(a), 12(b), and 12(c). The results show that when the NCAP is in a positive phase over decadal timescales, north China is affected by the anomalous water vapor flux transported from south to north; the direction of the anomalous water vapor flux transmission is opposite when the NCAP is in a negative phase over decadal timescales. The regression pattern of the vertically integrated whole layer water vapor flux anomalies against the negative NAT over decadal timescales shows that the anomalous water vapor flux transmission associated with the negative NAT correspond to that when the NCAP decadal variability is in a positive phase (Fig. 12(d)). These verify the dynamical linkage of the NAT to NCAP from the perspective of water vapor flux.

Here, the dynamical linkage between the NAT and NCAP over decadal timescales can be summarized as follows: the NAT can first stimulate upper-level convergence and divergence over the North Atlantic and then influence local atmosphere circulation over north China and its surrounding regions via the EAT pattern, so as to regulate the water vapor transport in north China, and finally influence the NCAP.

5 Physics-based prediction model for decadal NCAP

As mentioned above, it is of great significance to predict the NCAP in advance. In Section 3 and Section 4, the NCAP decadal variability with a cycle of about 10-year and the dynamical linkage between the NAT and NCAP over decadal timescales were explored. Here, a prediction model for decadal NCAP based on July NAT is established as follows:

$$\widetilde{\mathrm{NCAP}}^{*}(t) = a_1 \cdot \mathrm{July\ NAT}(t) + b_1 t + c_1, \qquad (10)$$

where $\widetilde{\mathrm{NCAP}}^{*}$ denotes the modeled NCAP decadal variability after removing the multidecadal trend, t denotes time in years, the coefficients a_1, b_1, and c_1 are determined empirically by multiple linear regression based on the least square method.

Figure 13(a) shows the observed and modeled NCAP decadal variability in which the multidecadal trend was removed for the period of 1979–2021. The detrended decadal NCAP model (Eq. (10)) was established based on observed values for NCAP and the July NAT index from 1979 to 2021. It can be seen that this model can well simulate the decadal variability of the NCAP, such as the increasing trend of the NCAP in the period of 1979–1983, 1990–1995, 2015–2020, and the decreasing trend in the period of 1985–1990, 1996–2002, 2010–2014. The

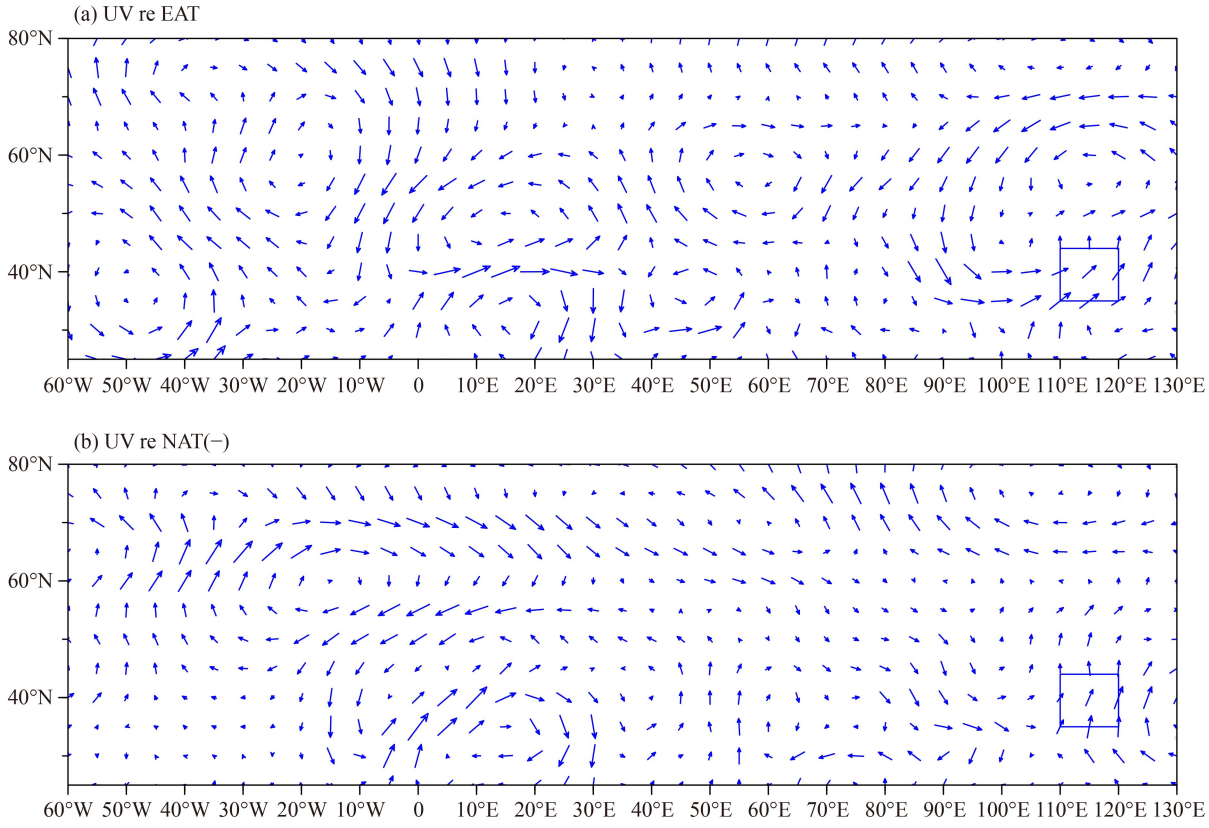

Fig. 11 Regression coefficients of the 500 hPa zonal-meridional wind against EAT index and negative NAT. (a) As in Fig. 7(a), but for the zonal-meridional wind. (b) As in (a), but against negative NAT [NAT(-)].

correlation coefficient between the observed and modeled NCAP decadal variability is 0.784 at a confidence level exceeding 98%. The root-mean-square error for the observed and modeled decadal NCAP is 7.5, which is very small compared with the variance of the NCAP decadal variability. As shown in Fig. 13(b), in order to analyze the influence of the multidecadal trend on the results of this model, a model including the multidecadal trend was established as follows:

$$\tilde{\text{NCAP}}(t) = a_2 \cdot \text{July NAT}(t) + b_2 t + c_2 + d_2 t, \qquad (11)$$

where $\tilde{\text{NCAP}}$ denotes the modeled NCAP decadal variability with the multidecadal trend included, the coefficients a_2, b_2, and c_2 are determined empirically as in Eq. (10), and the d_2 denotes the multidecadal trend of the NCAP. The results show that the multidecadal trend does not influence the simulations from this model.

To test the prediction skill of this decadal NCAP model, Fig. 14 shows the hindcasted experiments. As shown in Fig. 14(a), the decadal NCAP model without multidecadal trend was established based on the observed NCAP ang July NAT for the period of 1979–2016, 1979–2017, 1979–2018, 1979–2019, and 1979–2020, to predict the decadal NCAP in 2017, 2018, 2019, 2020, and 2021, respectively. To save figure space, these are all placed in one figure. The results show that this model has good hindcasted ability for the NCAP decadal variability, illustrating that this model can be applied to effectively predict the NCAP decadal variability. Figure 14(b), which considers multidecadal trend, shows similar results and will not be described in detail here.

These results indicate that the decadal NCAP model established based on the July NAT can effectively predict NCAP decadal variability. It also confirmed again the influences of the NAT on NCAP decadal variability, and the July NAT can be implicated as a predictor of the NCAP decadal variability.

6 Summary and discussion

In this paper we investigated NCAP decadal variability of a 10-year cycle, the mechanism of the NAT influencing the NCAP over decadal timescale, and a decadal NCAP model based on the July NAT.

The results indicate that NCAP has a decadal cycle of about 10-year superimposed on the multidecadal trend, and this is significantly negatively correlated with the July NAT over decadal timescales. Both the July NAT and NCAP have a decadal cycle of about 10-year. On decadal timescales, when the July NAT is in a negative phase, the NCAP anomalies without the multidecadal trend is in a positive phase, and vice versa. The correlation coefficient between the July NAT and NCAP

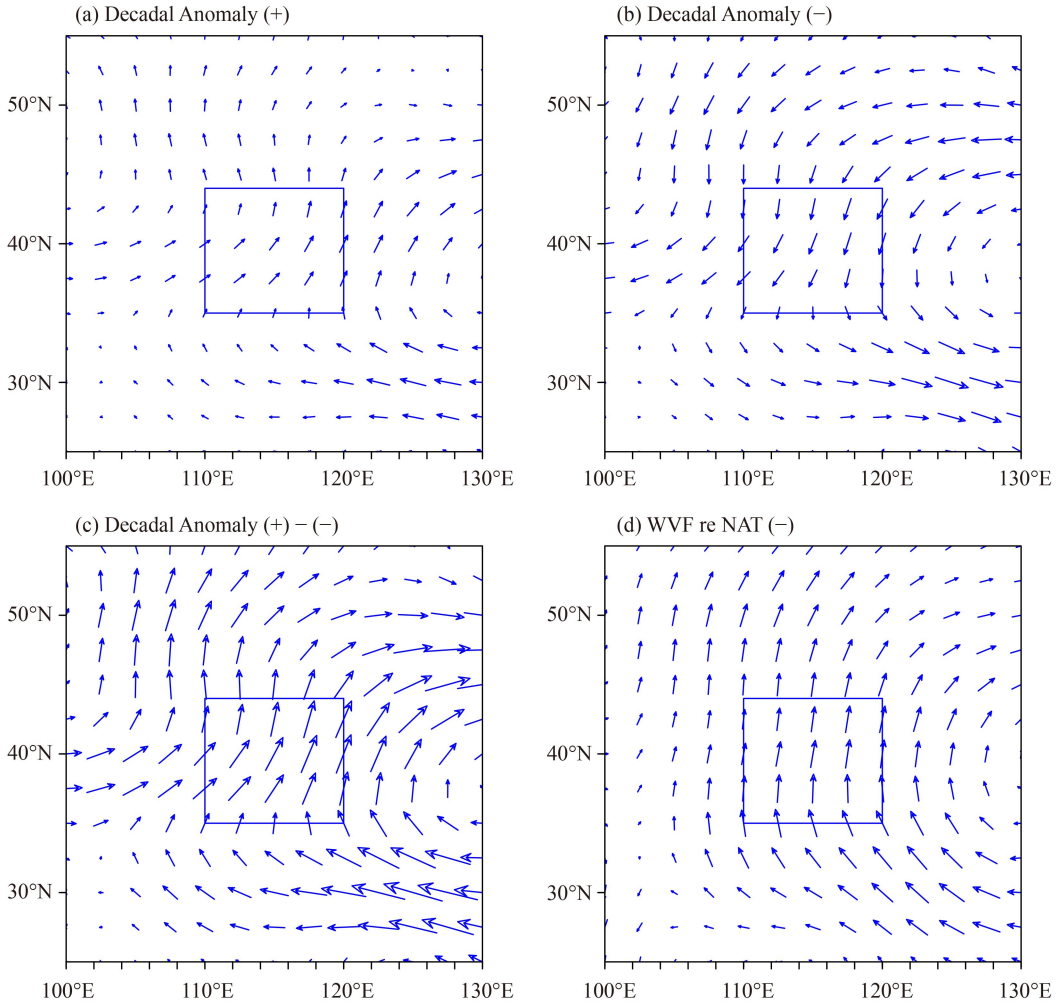

Fig. 12 Composite of August water vapor flux anomalies corresponding to the NCAP anomalies, its difference and regressing against negative NAT. (a) The composite of the vertically integrated whole water vapor flux anomalies in August during the period when the NCAP is in positive phase over decadal timescales. (b) As in (a), but for the period when the NCAP is in negative phase. (c) As in (a), but for the composite difference between (a) and (b). (d) The regression pattern of the vertically integrated whole layer water vapor flux anomalies over north China and the surrounding region onto the negative NAT over decadal timescales for 1979–2021.

over decadal timescales is –0.78 (exceeding the 95% significance level). The consistent results can also be obtained by the correlation coefficients map between the July NAT index ang the August precipitation anomalies over north China over decadal timescales. These indicate that the NAT may influence NCAP decadal variability and is a potential predictor for the decadal NCAP.

Based on the composite difference of the 500 hPa geopotential height field corresponding to NCAP decadal variability and the horizontal stationary wave activity flux corresponding to positive NCAP anomalies over decadal timescales. A decadal teleconnection in August defined as EAT pattern was found and the EAT pattern exhibits a distinct spatial structure in both the horizontal and vertical directions, with two positive and two negative activity centers over the North Atlantic-Eurasia region. The horizontal stationary wave activity flux that is associated with the EAT is almost consistent with that corresponding to the positive NCAP anomalies, illustrating that most of the atmospheric circulation field affecting the NCAP decadal variability is related to the EAT, and the EAT acts as an atmospheric bridge between the NAT and NCAP over decadal timescales.

Then, how the EAT is used as an atmospheric bridge between the NAT and NCAP over decadal timescales was further explored. Based on the results of this research and the analysis of previous studies (Han and Zhang, 2021), it is found that the August EAT can be stimulated by the cumulative effect of the NAT. The July NAT, August EAT, and NCAP reaches their significant lead-lag correlation at the same time on decadal timescale. In addition, the regression pattern of the wind anomalies at 500 hPa against the EAT index and the negative NAT on decadal timescales, respectively, and the analyses about the whole layer vertically integrated water vapor flux further support our conclusion: the EAT is an

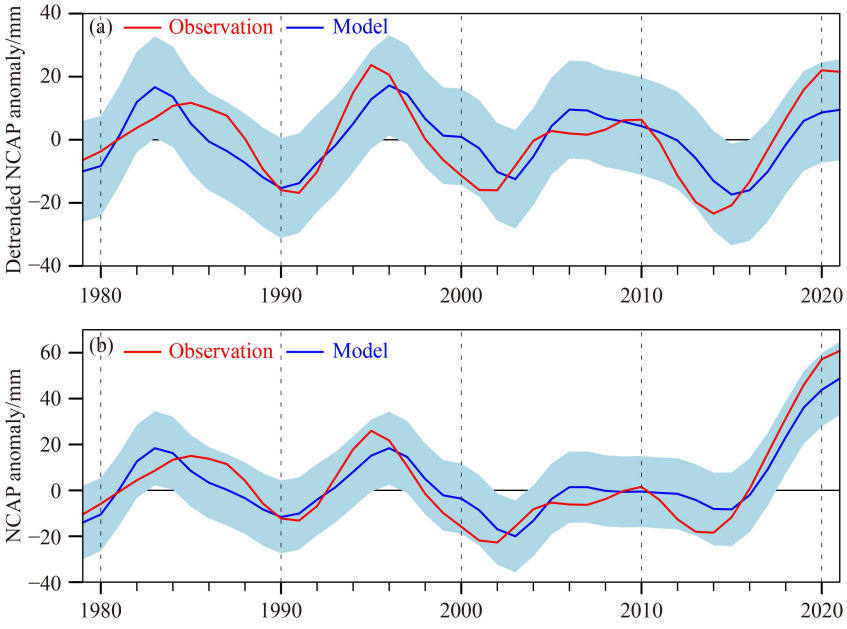

Fig. 13 Observed and modeled NCAP. (a) The red and blue lines are the observed and modeled detrended NCAP over decadal timescales for the period 1979–2021, respectively. The shaded areas indicate the 2-sigma uncertainty range of the modeled NCAP. (b) As in (a), but with the multidecadal trend included.

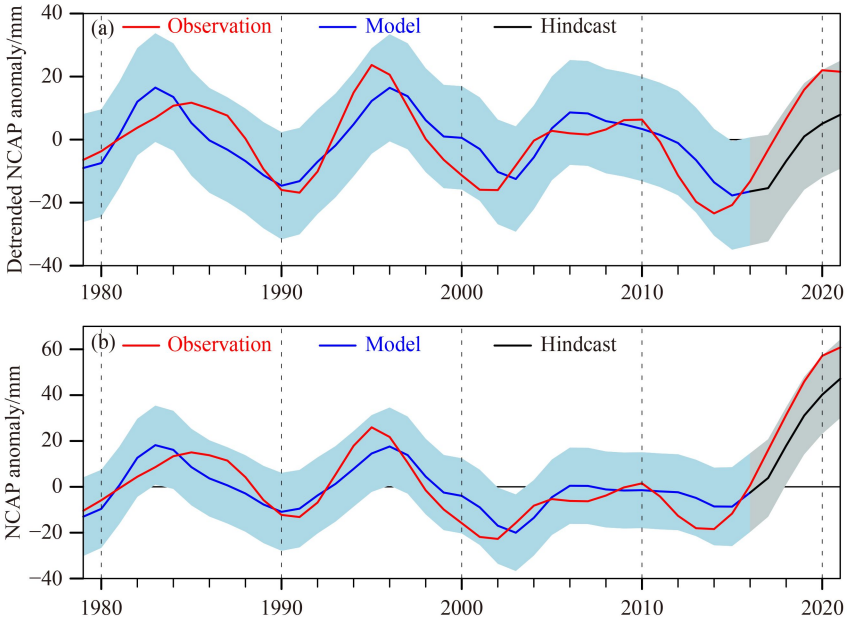

Fig. 14 Observed, modeled and hindcasted NCAP. (a) The red, blue and black lines are the observed, modeled and hindcasted detrended NCAP over decadal timescales, covering the period of 1979–2021, 1979–2016 and 2017–2021, respectively. The shaded areas indicate the 2-sigma uncertainty range for the modeled and hindcasted NCAP, respectively. (b) As in (a), but with the multidecadal trend included.

atmospheric bridge for the NAT influencing the decadal variability of the NCAP. When the July NAT is in a negative (positive) phase, the EAT pattern is in positive (negative) pattern which is conducive (unconducive) to the transmission of water vapor from the sea in the south-east to north China, thus increasing (decreasing) NCAP over decadal timescales.

Finally, a prediction model for decadal NCAP based on the July NAT is established. Through the analyses of the modeling and hindcasting, found that the decadal NCAP model established based on the July NAT can effectively predict NCAP decadal variability. These results also confirm again the influences of the NAT on NCAP decadal variability and show that the July NAT can be

implicated as a predictor of the NCAP decadal variability.

This research discusses the decadal variability of the NCJP about 10-year cycle and the dynamical linkage between the NAT and NCAP over decadal timescales. As shown in Fig. 1, there is also a multidecadal trend in NCAP, and whether this trend corresponds to the effect of global warming on precipitation deserves further exploration in the future. And, on the basis of the decadal and multidecadal variability, further work focused on exploring a predictor for annual NCAP variability would be helpful for improving NCAP prediction.

Acknowledgments This work was supported by the Innovation and development project of China Meteorological Administration (No. CXFZ2021J030). The authors wish to thank all the data providers and two reviewers.

References

Adler R F, Huffman G J, Chang A, Ferraro R, Xie P, Janowiak J, Rudolf B, Schneider U, Curtis S, Bolvin D, Gruber A, Susskind J, Arkin P, Nelkin E (2003). The version 2 Global Precipitation Climatology Project (GPCP) monthly precipitation analysis (1979–present). J Hydrometeorol, 4(6): 1147–1167

Bueh C, Li Y, Lin D, Lian Y (2016). Interannual variability of summer rainfall over the northern part of China and the related circulation features. J Meteorol Res, 30(5): 615–630

Chen P Y, Yu H, Xu M, Lei X T, Zeng F (2019). A simplified index to assess the combined impact of tropical cyclone precipitation and wind on China. Front Earth Sci, 13(4): 672–681

Choi K S, Kim B J, Zhang R H, Nam J C, Park K J, Kim J Y, Kim D W (2016). Possible influence of South Asian high on summer rainfall variability in Korea. Clim Dyn, 46(3–4): 833–846

Dai X G, Wang P, Chou J F (2003). Multiscale characteristics of the rainy season rainfall and interdecadal decaying of summer monsoon in north China. Chin Sci Bull, 48(24): 2730–2734

Ding Y H, Wang Z Y, Sun Y (2008). Inter-decadal variation of the summer precipitation in east China and its association with decreasing Asian summer monsoon. Part I: observed evidences. Int J Climatol, 28(9): 1139–1161

Fan K, Lin M J, Gao Y Z (2009). Forecasting the summer rainfall in north China using the year-to-year increment approach. Sci China Ser D Earth Sci, 52(4): 532–539

Fu C B, Zeng Z M (2005). Correlations between North Atlantic Oscillation Index in winter and eastern China Flood/Drought Index in summer in the last 530 years. Chin Sci Bull, 50(21): 2505–2516

Fu J J, Li S L, Luo D H (2009). Impact of global SST on decadal shift of East Asian summer climate. Adv Atmos Sci, 26(2): 192–201

Gill A E (1982). Atmosphere–Ocean Dynamics. New York: Academic

Hao L S, Ding Y H (2012). Progress of precipitation research in north China. Prog Geogr, 31(5): 593–601 (in Chinese)

Han J P, Zhang R H (2022). Influence of preceding North Atlantic Oscillation on the spring precipitation in the middle and lower reaches of the Yangtze River Valley. Int J Clim

Huang R H, Chen J L, Huang G (2007). Characteristics and variations of the East Asian monsoon system and its impacts on climate disasters in China. Adv Atmos Sci, 24(6): 993–1023

Jiang X W, Li Y Q, Yang S, Wu R G (2011). Interannual and interdecadal variations of the South Asian and western Pacific subtropical highs and their relationships with Asian-Pacific summer climate. Meteorol Atmos Phys, 113(3–4): 171–180

Jiang Z, Yang S, He J, Li J, Liang J (2008). Interdecadal variations of East Asian summer monsoon northward propagation and influences on summer precipitation over east China. Meteorol Atmos Phys, 100(1–4): 101–119

Kanamitsu M, Ebisuzaki W, Woollen J, Yang S K, Hnilo J J, Fiorino M, Potter G L (2002). NCEP–DOE AMIP-II reanalysis (R-2). Bull Am Meteorol Soc, 83(11): 1631–1644

Li C Y, Li G L (2000). The NPO/NAO and interdecadal climate variation in China. Adv Atmos Sci, 17(4): 555–561

Li X D, Zhu Y F, Qian W H (2002). Spatiotemporal variations of summer rainfall over eastern China during 1880–1999. Adv Atmos Sci, 19(6): 1055–1068

Li J P, Ren R C, Qi Y Q, Wang F M, Lu R Y, Zhang P Q, Jiang Z H, Duan W S, Yu F, Yang R Z (2013). Progress in air-land-sea interactions in Asia and their role in global and Asian climate change. Chin J Atmos Sci, 37(2): 518–538 (in Chinese)

Li G, Chen J, Wang X, Luo X, Yang D Y, Zhou W, Tan Y K, Yan H M (2018). Remote impact of North Atlantic sea surface temperature on rainfall in southwestern China during boreal spring. Clim Dyn, 50(1–2): 541–553

Li J P, Ruan C Q (2018). The North Atlantic–Eurasian teleconnection in summer and its effects on Eurasian climates. Environ Res Lett, 13(2): 024007

Li J P, Zheng F, Sun C, Feng J, Wang J (2019). Pathways of influence of the northern hemisphere mid-high latitudes on East Asian climate: a review. Adv Atmos Sci, 36(9): 902–921

Li J P, Xie T J, Tang X X, Wang H, Sun C, Feng J, Zheng F, Ding R Q (2022). Influence of the NAO on wintertime surface air temperature over East Asia: multidecadal variability and decadal prediction. Adv Atmos Sci, 39(4): 625–642

Lin Z D, Lu R Y (2009). The ENSO's effect on eastern China rainfall in the following early summer. Adv Atmos Sci, 26(2): 333–342

Liu Y Q, Ding Y H, Li Y H (1992). Transport of water vapor over north China during the drought period in summer of 1980. Adv Atmos Sci, 9(2): 213–222

Lu R Y (1999). Interdecadal variations of precipitations in various months of summer in north China. Plateau Meteorol, 18(4): 509–519 (in Chinese)

Lu R Y, Dong B, Ding H (2006). Impact of the Atlantic Multidecadal Oscillation on the Asian summer monsoon. Geophys Res Lett, 33(24): L24701

Mao J Y, Wu G X (2006). Intraseasonal variations of the Yangtze rainfall and its related atmospheric circulation feature during the 1991 summer. Clim Dyn, 27(7–8): 815–830

Pyper B J, Peterman R M (1998). Comparison of methods to account for autocorrelation in correlation analyses of fish data. Can J Fish Aquat Sci, 55(9): 2127–2140

Rayner N A, Parker D E, Horton E B, Folland C K, Alexander L V, Rowell D P, Kent E C, Kaplan A (2003). Global analyses of sea

surface temperature, sea ice, and night marine air temperature since the late nineteenth century. J Geophys Res, 108(D14): 4407

Sun C, Li J P, Jin F F (2015). A delayed oscillator model for the quasi-periodic multidecadal variability of the NAO. Clim Dyn, 45(7–8): 2083–2099

Sun C, Li J P, Ding R Q, Jin Z (2017). Cold season Africa–Asia multidecadal teleconnection pattern and its relation to the Atlantic multidecadal variability. Clim Dyn, 48(11–12): 3903–3918

Sun W G, Chen B Y, Guo Q (2009). Influence of the subtropical high over western Pacific on the difference between precipitation and evaporation in north China. Plateau Meteorol, 28(5): 1167–1174 (in Chinese)

Sun W, Li J, Yu R C, Yuan W H (2018). Circulation structures leading to propagating and non-propagating heavy summer rainfall in central north China. Clim Dyn, 51(9–10): 3447–3465

Takaya K, Nakamura H (2001). A formulation of a phase-independent wave-activity flux for stationary and migratory quasigeostrophic eddies on a zonally varying basic flow. J Atmos Sci, 58(6): 608–627

Wang B, Wu Z W, Li J P, Liu J, Chang C P, Ding Y, Wu G (2008). How to measure the strength of the East Asian summer monsoon. J Clim, 21(17): 4449–4463

Wei W (2012). The Meridional Variation and the Zonal Variation of the South Asian High. Dissertation for the Doctoral Degree. Beijing: Chinese Academy of Meteorological Sciences (in Chinese)

Wei W, Zhang R, Wen M, Rong X, Li T (2014). Impact of Indian summer monsoon on the South Asian High and its influence on summer rainfall over China. Clim Dyn, 43(5–6): 1257–1269

Wu R, Hu Z Z, Kirtman B P (2003). Evolution of ENSO-related rainfall anomalies in East Asia. J Clim, 16(22): 3742–3758

Wu Z W, Wang B, Li J P, Jin F F (2009). An empirical seasonal prediction model of the East Asian summer monsoon using ENSO and NAO. J Geophys Res, 114(D18): D18120

Wu R G, Jiao Y (2017). The impacts of the Indian summer rainfall on north China summer rainfall. Asia-Pac J Atmospheric Sci, 53(2): 195–206

Xie T J, Li J P, Sun C, Ding R Q, Wang K C, Zhao C F, Feng J (2019). NAO implicated as a predictor of the surface air temperature multidecadal variability over East Asia. Clim Dyn, 53(1–2): 895–905

Xie T J, Li J P, Chen K Q, Zhang Y Z, Sun C (2021). Origin of Indian Ocean multidecadal climate variability: role of the North Atlantic Oscillation. Clim Dyn, 56(9–10): 3277–3294

Xu G Y, Yang X Q, Sun X G (2005). Interdecadal and interannual variation characteristics of rainfall in north China and its relation with the northern hemisphere atmospheric circulations. Chin J Geophys, 48(3): 511–518 (in Chinese)

Xue F, Liu C (2008). The influence of moderate ENSO on summer rainfall in eastern China and its comparison with strong ENSO. Chin Sci Bull, 53(5): 791–800

Zhang Q Y, Tao S Y, Chen L T (2003). The interannual variability of East Asian summer monsoon indices and its association with the pattern of general circulation over East Asia. Acta Meteorol Sin, 61(5): 559–568

Zhang R H (1999). The role of Indian summer monsoon water vapor transportation on the summer rainfall anomalies in the northern part of China during the El Niño mature phase. Plateau Meteorol, 18(4): 567–574 (in Chinese)

Zhang R H (2015). Changes in East Asian summer monsoon and summer rainfall over eastern China during recent decades. Sci Bull, 60(13): 1222–1224

Zhao Y, Chen D L, Li J, Chen D D, Chang Y, Li J, Qin R (2020). Enhancement of the summer extreme precipitation over north China by interactions between moisture convergence and topographic settings. Clim Dyn, 54(5–6): 2713–2730

Zhao T T G, Zhao J S, Hu H C, Ni G H (2016). Source of atmospheric moisture and precipitation over China's major river basins. Front Earth Sci, 10(1): 159–170

Zhu J H, Wang S W (2001). 80a-oscillation of summer rainfall over east of China and east Asian summer monsoon. Adv Atmos Sci, 18(5): 1043–1051

Zuo J Q, Li W J, Sun C H, Xu L, Ren H L (2013). Impact of the North Atlantic sea surface temperature tripole on the East Asian summer monsoon. Adv Atmos Sci, 30(4): 1173–1186